Refractive index and temperature optical fiber sensor based on thin core S-taper and spherical structure*

YANG Fan[1], CAO Ye[1], LI Meiqi[1], JU Hui[1], and LI Lijun[2]**

1. School of Electronic and Information, Qingdao University, Qingdao 266071, China

2. College of Electronic Information Engineering, Shandong University of Science and Technology, Qingdao 266590, China

(Received 25 September 2021; Revised 22 December 2021)

A Mach-Zehnder interferometer (MZI) for simultaneously measuring refractive index (RI) and temperature is proposed and verified in this paper. The sensor head is composed of thin core fiber (TCF) S-taper structure and spherical structure. By monitoring two interference dips, experimental results show that the RI sensitivities are −70.392 nm/RIU and −60.08 nm/RIU in the RI range of 1.338 4—1.350 0, respectively. And the temperature sensitivities are 0.050 72 nm/°C and 0.071 7 nm/°C in the temperature range of 30—70 °C, respectively. The simultaneous measurement of the temperature and external RI is demonstrated based on the sensitive matrix. The sensor also has the advantages of low cost, simple structure and high sensitivity.

Document code: A **Article ID:** 1673-1905(2022)06-0321-5

DOI https://doi.org/10.1007/s11801-022-1153-3

Optical fiber sensors have been widely used in many fields such as physics, chemistry, biology and so on, because of their unique advantages of low transmission loss, small size and simple fabrication. The traditional coupling structures used to construct Mach-Zehnder interferometers (MZIs) include single mode-multimode-single mode (SMS) structure[1], core-offset structure[2], taper structure[3], fiber grating[4], etc, which are exploited to monitor temperature[5], humidity[6], strain[7], magnetic field[8], refractive index (RI)[9] and other parameters. In recent years, S-taper has attracted numerous research interest due to its low cost, compactness, and good fiber compatibility. In 2015, LIU et al[10] presented an optical fiber humidity sensor based on the S-taper fiber coated with SiO_2 nanoparticles, whose wavelength and intensity sensitivities reach 1.171 8 nm/%RH and 0.441 dB/%RH, respectively. In 2018, CHEN et al[11] proposed an RI sensor based on the reflection-type S-taper with a sensitivity up to 268.8 nm/RIU. In the same year, ZHAO et al[12] proposed an S-taper cascaded on fiber Bragg grating (FBG) sensor with a maximum RI sensitivity of 269.76 dB/RIU. In 2020, LI et al[13] fabricated an optical fiber sensor based on an S-taper embedded in long-period grating for measurement of strain and temperature, whose sensitivities reach 53.6 pm/με and 70 pm/°C, respectively. With the rapid development of optical fiber sensing technology, a variety of new structures and technologies were proposed[14,15]. The research of interferometric optical fiber sensor is more in-depth and diversified.

In this paper, an MZI based on thin core S-taper and spherical structure for simultaneous measurement of RI and temperature is proposed. Thin core fiber (TCF) has weak light binding ability, which is more likely to excite higher-order cladding mode. Compared with the S-taper structure made on the traditional single-mode fiber, the S-taper structure made on the TCF integrates the advantages of these two components. The transmission spectrum will shift with the variation of temperature and RI. The sensitivity of RI and temperature can be calculated respectively based on the shift of spectrum, and the simultaneous measurement of the temperature and external RI is demonstrated based on the sensitive matrix. The sensor has the advantages of simple structure, small size and high sensitivity. It would be widely used in physical, chemical and biological sensing fields.

The schematic diagram of the proposed sensor is shown in Fig.1. The sensing structure is composed of S-taper in the TCF cascaded spherical structure. Because of the weak confinement ability of the TCF to light, the S-taper structure located in the TCF is easier to excite the cladding mode. The spherical structure partially couples the cladding mode from the TCF back to the fiber core, and the mode interference will appear at the output end of the cascaded fiber structure.

The fabrication method of spherical structure is arc discharge. A segment of single-mode fiber with the coating layer removed is fixed in the central discharge

* This work has been supported by the National High Technology Research and Development Program of China (No.2013AA014200), the National Natural Science Foundation of China (No.11444001), and the Municipal Natural Science Foundation of Tianjin (No.14JCYBJC16500).

** E-mail: cynever@163.com

part of the fusion splicer. The discharge intensity is 200 bit, and the discharge mode is set to “arc”. A spherical structure is obtained after one discharge.

The thin-core S-taper is also manufactured by applying electrical discharge on the TCF using a fiber fusion splicer. First, the manual splicing mode of the fusion splicer is chosen, and the left and right motors of the fusion splicer are adjusted to achieve the minimum distance between the two. A segment of TCF with the coating layer removed is placed on the fusion splicer. Second, the lateral offset in the *x*-direction is introduced by manually modulating the movement of one fiber clamp. The discharge mode is set to "clean mode" and the discharge intensity is set to 85. The discharge operation of the TCF is started. After one discharge, the left and right motors of the fusion splicer are manually controlled to make the TCF in a straightened state again. The above operations are repeated until thin-core S-taper with ideal geometric parameters could be acquired. Finally, the thin core S-taper and spherical structure are spliced together with fiber fusion splicer.

In this experiment, the parameters of thin core S-taper and spherical fiber are as follows. The core and cladding diameters of TCF are 5 μm and 125 μm, respectively. W_1 is the waist diameter of thin core S-taper, W_1=98.7 μm. L_1 is the length of taper, L_1=441.3 μm. Δd is the displacement, Δd=27.9 μm. W_2 is a spherical diameter, W_2=149.7 μm. The micrographs of the thin core S-taper structure and the spherical structure are shown in Fig.2.

Fig.3 describes the simulation of the beam propagation field in the sensing structure according to the beam propagation method (BMP). It can be seen from the simulation that because of the thin core S-taper is used as a beam splitter, when the incident light just enters the S-taper, part of the light will be coupled into the cladding to excite the cladding modes, resulting in the light intensity weakening in the core. As the light continues to propagate in the S-taper, a small part of the cladding modes light will be coupled back to the core due to the structure effect, resulting in the increase of light intensity in the core. When the light reaches the spherical structure, part of the cladding modes excited by the thin core S-taper are coupled back to the core. Due to the phase difference between the fiber modes, mode interference occurs.

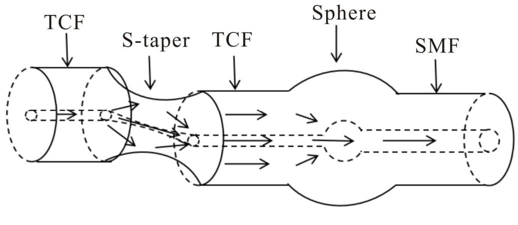

Fig.1 Schematic diagram of the proposed sensor

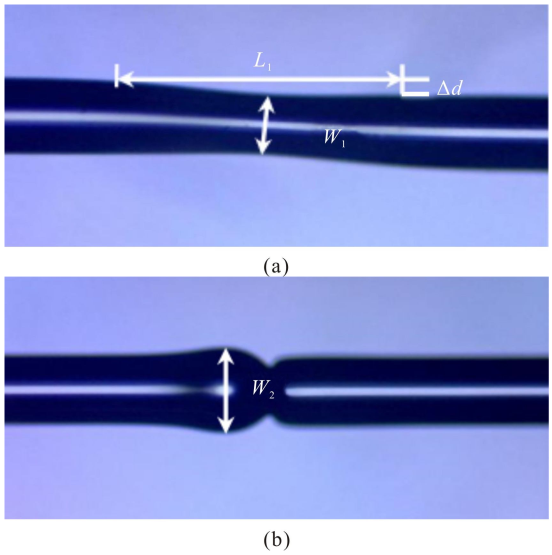

Fig.2 (a) The micrograph of the S-taper structure; (b) The micrograph of the spherical structure

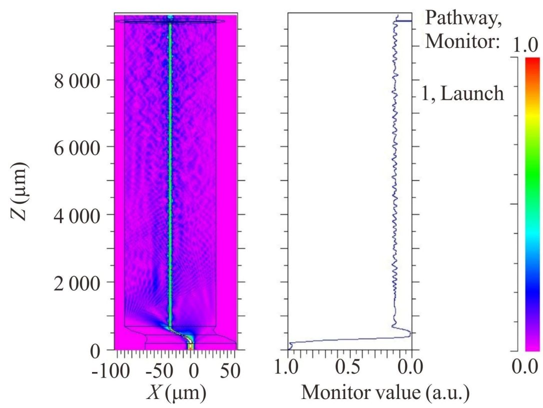

Fig.3 Simulated optical field distribution of the sensor

The transmission light intensity of the studied sensor is described as

$$I = I_{\text{core}} + I_{\text{clad}} + 2\sqrt{I_{\text{core}} \cdot I_{\text{clad}}} \cos\Delta\varphi, \tag{1}$$

where I is the output intensity of the studied sensor, and I_{core} and I_{clad} are the intensities of the core and cladding modes, respectively. $\Delta\varphi$ is the phase difference between core mode and the m-order cladding mode, which can be expressed as

$$\Delta\varphi = \frac{2\pi}{\lambda}\left(n_{\text{core}} - n_{\text{clad}}\right)L = \frac{2\pi}{\lambda}\Delta n_{\text{eff}} L\,, \tag{2}$$

where n_{core} and n_{clad} represent the effective indices of core mode and the m-order cladding mode in TCF, respectively, Δn_{eff} is the difference of effective RI between core mode and cladding mode, λ is the wavelength, and L is the length of the interference arm. When $\Delta\varphi=(2k+1)\pi$ with k=0, 1, 2, 3,.... The wavelength at the interference dip can be expressed as

$$\lambda_{\text{D}} = 2\Delta n_{\text{eff}} L / \left(2k+1\right). \tag{3}$$

When the external RI of the sensor changes, the n_{clad} would alter correspondingly, but n_{core} has almost no change, so the Δn_{eff} would alter. According to Eq.(3), it is obvious that the dip wavelength would shift.

Transmission spectral characteristics may be also sensitive to the variation of environment temperature owing to thermo-optic and thermal expansion effects. As the ambient temperature increases, both n_{clad} and n_{core} increase. The n_{core} changes more, since the thermo-optic coefficient of fiber core is higher than that of the fiber cladding[16]. In addition, the interference length will also increase due to the thermal expansion effect of the fiber. So the Δn_{eff} and L would both increase. According to Eq.(3), it is obvious that the dip wavelength would show some red shift with the increase in temperature.

Therefore, we can measure the change of temperature and RI by monitoring the shift of the dip wavelength of the interferometer.

Fig.4 shows the sensing system of measuring RI. The experimental system mainly includes an optical spectrum analyzer (OSA, AQ6370) and a broadband light source (BBS) with a range from 1 250 nm to 1 640 nm.

The NaCl solutions with different concentrations are prepared as the RI samples, and the RI of the solutions varies from 1.338 4 to 1.350 0, which are certified by an Abbe refractometer. The sensor structure is immersed into the NaCl solutions with different concentrations, and the two ends of the sensor are connected to the BBS and the OSA. The transmission spectra of the sensor are recorded by OSA. After the output spectrum was recorded, the sensor structure was cleaned with 99% industrial ethanol and deionized water and dried. The procedure was repeated to measure the other RI solutions.

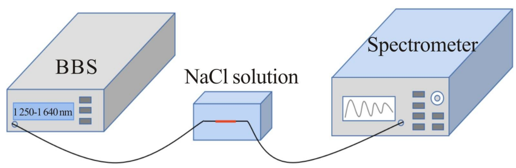

Fig.4 Schematic diagram of the proposed RI sensing system

Fig.5 shows the changes in transmission spectrum with the RI range of 1.338 4—1.350 0. As the RI increases, the wavelengths of dip1 and dip2 have a blue shift. Since the n_{clad} is very sensitive to the change of the external environment RI, the n_{clad} increases with the increase of the external environment RI, which causes the Δn_{eff} decreases. According to Eq.(3), the interference dips wavelength drifts to the direction of short wavelength.

The RI responses of the studied sensor at two dips are shown in Fig.6. For dip1, the wavelength shifts from 1 589.81 nm to 1 588.92 nm with a change of 0.89 nm, and the RI sensitivity is −70.392 nm/RIU with a good linearity of R^2=0.977 9. For dip2, the wavelength shifts from 1 602.87 nm to 1 602.13 nm with a change of 0.74 nm, and the RI sensitivity is −60.08 nm/RIU with a good linearity of R^2=0.990 4.

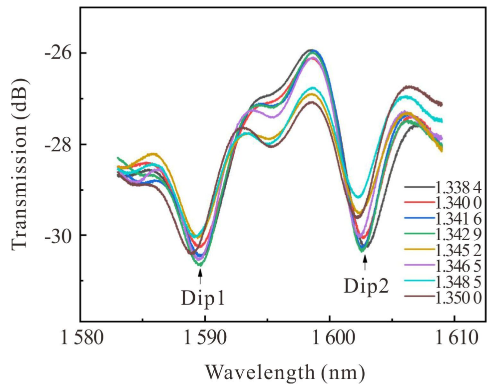

Fig.5 Transmission spectra of the sensing structure with different RIs

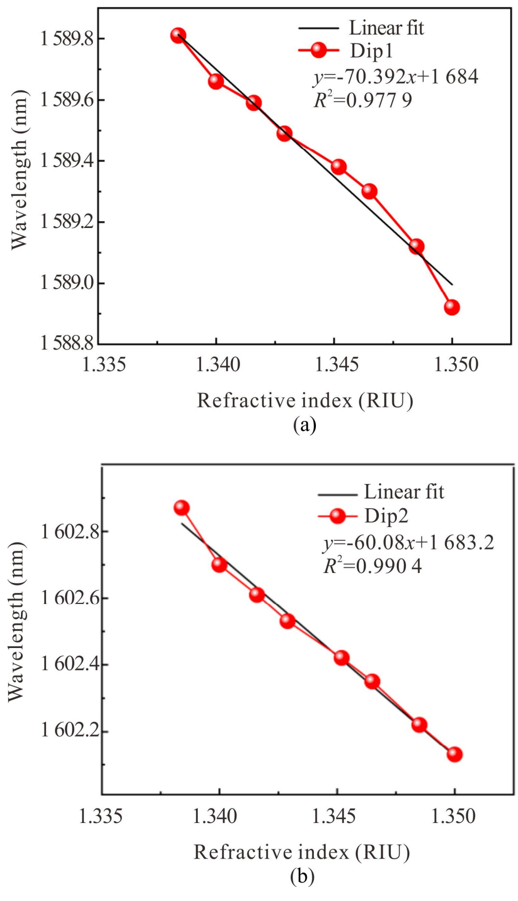

Fig.6 RI response characteristics of the (a) dip1 and (b) dip2

Fig.7 shows the schematic diagram of the temperature sensing system. The structure of optical fiber sensor is fixed in the temperature controller. The external temperature gradually rises from 30 °C to 70 °C, and the change of the transmission spectrum is recorded for every 5 °C change.

The transmission spectra of the sensor with different temperatures are shown in Fig.8. It shows that the output spectrum shifts towards long wavelength with temperature increasing from 30 °C to 70 °C.

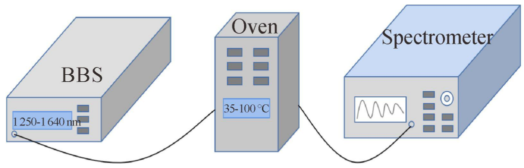

Fig.7 Schematic diagram of the proposed temperature sensing system

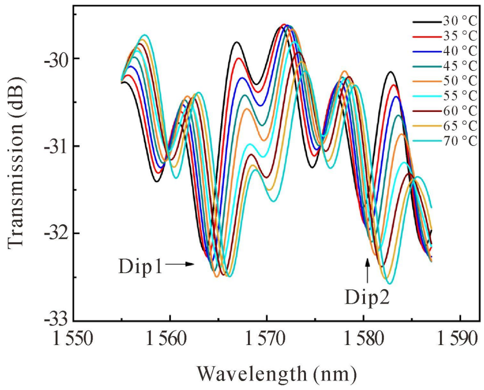

Fig.8 Transmission spectra of the sensing structure at different temperatures

The temperature responses of the studied sensor at two dips are shown in Fig.9. For dip1, the wavelength shifts from 1 563.62 nm to 1 566.19 nm with a change of 2.57 nm, and the temperature sensitivity is 0.050 72 nm/°C with a good linearity of R^2=0.998 4. For dip2, the wavelength varies by about 2.79 nm, and the RI sensitivity is 0.071 7 nm/°C with a good linearity of R^2=0.997 2.

It is easy to know that the RI sensitivity and temperature sensitivity at dip1 are different from those at dip2. The shifts of dip1 and dip2 arisen by RI and temperature can be described as

$$\begin{bmatrix}\Delta\lambda_{\text{dip1}}\\ \Delta\lambda_{\text{dip2}}\end{bmatrix}=\begin{bmatrix}K_{T,\text{dip1}} & K_{R,\text{dip1}}\\ K_{T,\text{dip2}} & K_{R,\text{dip2}}\end{bmatrix}\begin{bmatrix}\Delta T\\ \Delta R\end{bmatrix}, \tag{4}$$

where $\Delta\lambda_{\text{dip1}}$ and $\Delta\lambda_{\text{dip2}}$ refer to wavelength shifts of dip1 and dip2, respectively. And ΔT and ΔR respectively represent the variations of environmental temperature and RI. Temperature sensitivity and RI sensitivity of dip1 are represented by $K_{T,\text{dip1}}$ and $K_{R,\text{dip1}}$, respectively. $K_{T,\text{dip2}}$ and $K_{R,\text{dip2}}$ express the temperature sensitivity and RI sensitivity of dip2, respectively.

All the sensitivity coefficients have been obtained from the experimental results. We can use a sensitivity matrix to obtain the variation in temperature and RI. The sensitivity matrix is given as

$$\begin{bmatrix}\Delta T\\ \Delta R\end{bmatrix}=\frac{1}{D_1}\begin{bmatrix}K_{R,\text{dip2}} & -K_{R,\text{dip1}}\\ -K_{T,\text{dip2}} & K_{T,\text{dip1}}\end{bmatrix}\begin{bmatrix}\Delta\lambda_{\text{dip1}}\\ \Delta\lambda_{\text{dip2}}\end{bmatrix}, \tag{5}$$

where $D_1=K_{T,\text{dip1}}K_{R,\text{dip2}}-K_{T,\text{dip2}}K_{R,\text{dip1}}$. Then substitute the experimental data into Eq.(5), and we get

$$\begin{bmatrix}\Delta T\\ \Delta R\end{bmatrix}=\frac{1}{2}\begin{bmatrix}-60.08 & 70.392\\ -0.071\,7 & 0.050\,72\end{bmatrix}\begin{bmatrix}\Delta\lambda_{\text{dip1}}\\ \Delta\lambda_{\text{dip2}}\end{bmatrix}. \tag{6}$$

Therefore, the cascaded device composed of thin core S-taper and spherical structure can be used to measure the changes of the environmental temperature and RI simultaneously.

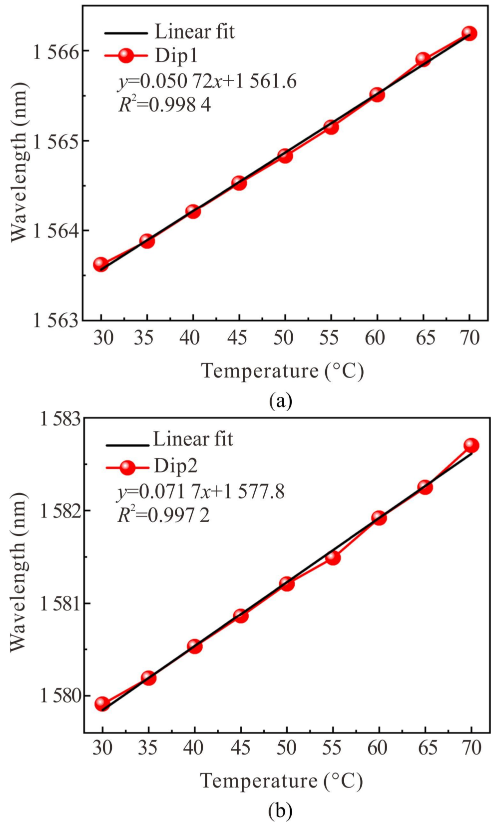

Fig.9 Temperature response characteristics of the (a) dip1 and (b) dip2

In conclusion, an optical fiber sensor based on the thin core S-taper and spherical structure is proposed, both RI and temperature characteristics of this sensor are experimentally investigated. The two selected interference dips exhibit different sensing characteristics, so simultaneous measurement of temperature and RI can be achieved by calculating the sensing coefficient matrix. The RI sensitivities of the two dips are −70.392 nm/RIU and −60.08 nm/RIU, and the temperature sensitivities of the two dips are 0.050 72 nm/°C and 0.071 7 nm/°C. In addition, the proposed sensor has good stability and repeatability, which is suitable for practical production applications without complex fabrication.

Statements and Declarations

The authors declare that there are no conflicts of interest related to this article.

References

[1] WU Q, SEMENOVA Y, WANG P, et al. High sensitivity SMS fiber structure based refractometer–analysis and experiment[J]. Optics express, 2011, 19(9): 7937-7944.

[2] CAO Y, LIU H, TONG Z R, et al. Simultaneous measurement of temperature and refractive index based on a core-offset Mach-Zehnder interferometer cascaded with a long-period fiber grating[J]. Optoelectronics letters, 2015, 11(1)：69-72.
[3] GAO S C, ZHANG W G, GENG P C, et al. Highly sensitive in-fiber refractive index sensor based on down-bitaper seeded up-bitaper pair[J]. IEEE photonics technology letters, 2012, 24(20)：1878-1881.
[4] MA G M, JIANG J, MU R D, et al. High sensitive FBG sensor for equivalent salt deposit density measurement[J]. IEEE photonics technology letters, 2014, 27(2)：177-180.
[5] LIU Q, WANG S W, FU X H, et al. Refractive index insensitive temperature sensor based on waist-enlarged few mode fiber bitapers[J]. Optoelectronics letters, 2017, 13(1)：25-28.
[6] WANG Y Q, SHEN C Y, LOU W M, et al. Fiber optic relative humidity sensor based on the tilted fiber Bragg grating coated with graphene oxide[J]. Applied physics letters, 2016, 109(3)：031107.
[7] TIAN K, ZHANG M, FARRELL G, et al. Highly sensitive strain sensor based on composite interference established within S-tapered multimode fiber structure[J]. Optics express, 2018, 26(26)：33982-33992.
[8] WU W W, CAO Y, ZHANG H, et al. Compact magnetic field sensor based on a magnetic-fluid-integrated fiber interferometer[J]. IEEE magnetics letters, 2019, 10：1-5.
[9] ZHONG Y M, TONG Z R, SONG D Y, et al. Refractive index and temperature sensor based on cleaved taper and spherical structure[J]. Optoelectronics letters, 2020, 16(3)：171-175.
[10] LIU H F, MIAO Y P, LIU B, et al. Relative humidity sensor based on S-taper fiber coated with SiO_2 nanoparticles[J]. IEEE sensors journal, 2015, 15(6)：3424-3428.
[11] CHEN C, YANG R, ZHANG X Y, et al. Compact refractive index sensor based on an S-tapered fiber probe[J]. Optical materials express, 2018, 8(4)：919-925.
[12] ZHAO J F, NIU P P, ZHANG C, et al. Temperature-compensated fiber laser refractometer based on compact hybrid S-taper/FBG structure[J]. Optical fiber technology, 2018, 45：300-305.
[13] LI M Q, CAO Y, ZHANG H, et al. Strain and temperature sensor based on S-taper embedded in long-period grating[J]. Optical engineering, 2020, 59(9)：097105.
[14] YIN X L, ZHOU R X. Compact vector fiber-optic displacement sensor using an asymmetric Mach-Zehnder interferometer[J]. Optics communications, 2017, 400：74-78.
[15] DONG X R, DU H F, LUO Z, et al. Highly sensitive strain sensor based on a novel Mach-Zehnder interferometer with TCF-PCF structure[J]. Sensors, 2018, 18(1)：278.
[16] LI J L, ZHANG W G, GAO S C, et al. Long-period fiber grating cascaded to an S fiber taper for simultaneous measurement of temperature and refractive index[J]. IEEE photonics technology letters, 2013, 25(9)：888-891.